UCRL-JC-130104
PREPRINT

Experimental Measurements of Hydrodynamic Instabilities on Nova or Relevance to Astrophysics

S. G. Glendinning, K. S. Budil, C. Cherfils,
R. P. Drake, D. Farley, D. H. Kalantar,
J. Kane, M. M. Marinak, B. A. Remington,
A. Richard, D. Ryutov, J. Stone,
R. J. Wallace, and S. V. Weber

This paper was prepared for submittal to the
Second International Workshop on Laboratory Astrophysics with Intense Lasers
Tucson, Arizona
March 19-21, 1998

September 11, 1998

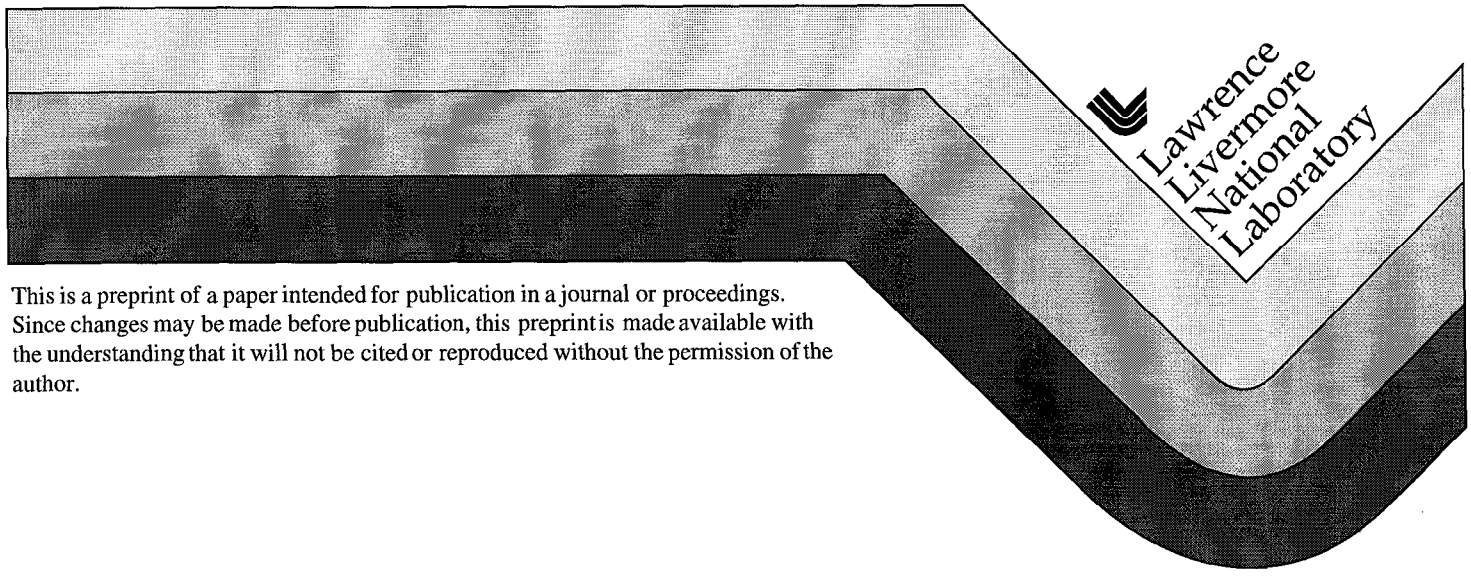

Experimental Measurements of Hydrodynamic Instabilities on Nova of Relevance to Astrophysics.

S.G.Glendinning[1], K.S.Budil[1], C.Cherfils[4], R.P.Drake[2], D.Farley[1], D.H.Kalantar[1], J.Kane[1], M.M.Marinak[1], B.A.Remington[1], A.Richard[4], D.Ryutov[1],J.Stone[3], R.J.Wallace[1], S.V.Weber[1]

[1]LLNL, [2]University of Michigan,[3]University of Maryland, [4]CEA-DRIF

Abstract: Large lasers such as Nova allow the possibility of achieving regimes of high energy densities in plasmas of millimeter spatial scales and nanosecond time scales. In those plasmas where thermal conductivity and viscosity do not play a significant role, the hydrodynamic evolution is suitable for benchmarking hydrodynamics modeling in astrophysical codes. Several experiments on Nova examine hydrodynamically unstable interfaces. A typical Nova experiment uses a gold millimeter-scale hohlraum to convert the laser energy to a 200 eV blackbody source lasting about a nanosecond. The x-rays ablate a planar target, generating a series of shocks and accelerating the target. The evolving areal density is diagnosed by time-resolved radiography, using a second x-ray source. Data from several experiments are presented and diagnostic techniques are discussed.

In inertial confinement fusion (ICF) implosions, energy (either from laser beams, particle beams, or x-rays) is deposited in the surface of a capsule, caus-

ing the surface material to be ablated and the residual material to be driven inward. At the ablation surface (where the material velocity changes direction), the pressure is decreasing toward the center of the capsule and the density is increasing; the surface is thus Rayleigh-Taylor (RT) unstable and modulations in velocity, density, or surface position will grow exponentially. In fact, too large an initial perturbation will fatally disrupt an implosion. Thus, RT growth at the ablation front in ICF-relevant conditions has been the subject of considerable study over the past two decades (Nuckolls et al. 1972; Kilkenny et al. 1994). One difference between classical RT instability and ablation front RT was apparent from the earliest years: ablation removes perturbed material from the surface, and this convection of vorticity significantly reduces the growth rate from classical values. The growth of perturbations in both the linear and (weakly) nonlinear regimes has been the subject of a variety of experiments performed on the Nova laser, among many other ICF facilities.

In laser-driven ablation front experiments, it is usually not possible to achieve pure RT growth, but rather a sequence of regimes, beginning with growth of a propagating perturbed shock, followed by combination of RT and, in planar geometry at least, decompression. Thus, direct comparison of experimental results with analytical expressions for pure RT or Richtmeyer-Meschkov growth is difficult and often confusing. We have taken the approach of comparing our experimental results primarily with detailed nu-

merical simulations which include the experimental conditions and, after benchmarking the codes used to the experiments, simulating pure (if difficult to achieve) regimes of hydrodynamic instabilities for comparison with analytical models.

It is possible using laser drive to drive planar foils(Glendinning et al. 1992; Remington et al. 1992; Weber et al. 1994), cylinders (Hsing et al. 1997), and spheres (i.e., capsules) (Landen et al. 1996) and hydrodynamic instabilities behave differently in each case. In addition, the modal dependence of an instability may be determined by experiments with single mode perturbations in one direction (a two-dimensional perturbation) and by examining the interaction of many modes. Finally, the mode structure may be made three-dimensional. In our experiments with the Nova laser, we have separately examined geometric effects on the ablation front RT instability: one-dimensional hydro in which we measure in planar or convergent geometry the position of vs. time of unperturbed foils or capsules, two-dimensional hydro (single- and many-mode perturbations), three-dimensional hydro (single- and many-mode bumps), and a single-mode perturbation in convergent geometry. In our experiments the initial perturbations are spatial variations, although experiments with pressure variations (induced by a nonuniform laser drive) are generally reported in the literature (Endo et al. 1995; Pawley et al. 1997).

In these proceedings we will describe two experiments from the Nova laser, one in planar geometry and one in convergent geometry. In the first experiment, we report the evolution of one-dimensional, two-dimensional single-mode, and three-dimensional multimode perturbations at the ablation front in planar foils, and in the second, we report our measurements of the growth of a single-mode perturbation on an imploding capsule. Our experiments are well modeled with 2- and 3- dimensional radiation hydrodynamics codes. We note that an RT unstable interface exists at photoevaporation fronts in astrophysical objects such as M16 (Hester et al. 1996). Codes used for modeling photoevaporation fronts may be applicable to our experiments, providing additional benchmarks for such codes.

The physics issues which must be addressed at the ablation front for our experimental conditions include: a highly collisional plasma (in general ln Λ, the collision logarithm, ~ 7), thus thermal transport and hydro motion take place by electron-electron, electron-ion, and ion-ion collisions; the deposition of X-ray energy in the plasma, both from drive and from self-emission; and the generation of multiple shocks at the ablation front and their propagation through unablated material. Usually the diffusion approximation is used to describe heat transport in our codes. Detailed equations of state of materials, rather than an ideal gas approximation, determine hydrodynamic behavior in shock compressed, unablated material.

In the Nova experiments, the main diagnostic is time-resolved two-dimensional radiography, typically in a face-on geometry, shown in Figures 1a and b (planar and convergent geometry, respectively). In this configuration, modulations in areal density are measured as modulations in backlighter x-ray intensity. For comparison with simulations, the code simulations are post-processed to predict intensity modulations. This requires detailed knowledge of the imaging diagnostic modulation transfer function (MTF) and the energy spectrum of the x-ray backlighter. On Nova, gated pinhole cameras are typically used as imaging diagnostics. The magnification is typically 4-12X, with 10 μm pinholes. The MTF of the framing camera and pinhole combination at 8X, the configuration used for these experiments, is shown in Figure 2 (Robey, Budil & Remington 1997). The instrument assembly is shown in Figures 3a and b. There are four active strips on a microchannel plate (MCP), each of which is activated by a high voltage pulse. Adjusting trombone lines sets the synchronicity of the four strip lines, and each stripline can be delayed independently. The gate width can be varied readily by changing the pulse forming modules, from between 200 ps and 1 ns (corresponding x-ray gate times are shorter, between 100 ps and 600 ps). The high voltage pulse to the microchannel plate is about 1.2 kV with no DC bias applied and both forward and reverse biases can be applied. Another very similar camera used on these experiments has frame times of 50 ps (Bradley et al. 1995).

Another diagnostic is frequently used when one-dimensional imaging as a function of time is required; this is the imaging x-ray streak camera(Remington et al. 1992). These streak cameras, as used on Nova, image using a slit typically 5-10 μm wide and 1.5 mm long. The image is formed onto a time-resolving slit perpendicular to the first.

The x-ray backlighters are produced by one or more Nova beams incident on solid targets (Glendinning et al. 1995). The planar experiment used a Sc backlighter (predominantly He-a lines at 4.3 keV) and the convergent experiment used Rh (various L-shell lines between 2.6 and 3.6 keV). The spectra were measured using crystal spectrometers and are shown in Figures 4a and b.

The two experiments used different shaped laser pulses to generate different x-ray drive histories. The planar experiment used a scale 1 Nova hohlraum, a gold cylinder 3000 μm long by 1600 μm in diameter. The 3.5 ns shaped laser drive and the resulting x-ray drive are shown in Figure 5a. The foil for this experiment was $C_{50}H_{47}Br_3$ (density 1.26 gm/cm^3, thickness about 60 μm) with modulations on the driven side. The convergent experiment used a similar scale 1 Nova hohlraum, and a 2.2 ns shaped laser drive pulse. The laser pulse and x-ray drive for this experiment are shown in Figure 5b. This experiment used a capsule, typically 400 μm inner diameter with a wall thickness of 35 μm plastic doped with 1.25% Ge. The capsules were not pressurized as in a

typical implosion experiment and were mounted in a hole on the side of the hohlraum. Again, the preimposed surface modulations faced the drive.

I. Three-dimensional planar experiments

The planar experiment examined (on separate shots): the motion of an unperturbed foil (side-on radiography with the x-ray streak camera); growth of 2D sinusoid perturbations as a function of time (face-on radiography with the x-ray framing camera); and growth of 3D multimode perturbations as a function of time (again, face-on radiography with the x-ray framing camera). The 2D sinusoid targets were produced by pressing plastic foils into machined molds, but the 3D targets required a mold which could not be produced by machining. This mold was produced by ablating a piece of Kapton with an excimer laser (Wallace, McEachern & Wilcox 1994); each "hit" from the laser produced a nearly Gaussian pit, and the sum of several hundred pits produced the designed pattern. This pattern, shown in Figure 6a, has reflective (cosine) symmetry about its center and a period of 300 μm. The pattern was continued beyond the 300 μm square by an additional 1/2 period on each side. A radiograph of the foil produced from this mold is shown in Figure 6b. The RMS amplitude produced in the foil was measured by contact profilometry to be about 0.66 μm.

The targets were driven with the hohlraums and experimental configurations described above. The unperturbed foil data was analyzed by determining the position of the leading-edge point of maximum change in transmission as a function of time from the streaked image. This result and the simulated result are shown in Figure 5a. Each of the 2D or 3D target shots were analyzed by the following process: 300 μm square (in the object plane) sections of each image were chosen for analysis; each frame was converted to film exposure; and the long scale length backlighter structure was removed by dividing out a second order two dimensional fit. The negative of the natural logarithm of the result is equivalent to optical depth (τ), and because the opacity of the shock heated material is nearly cold opacity (at the backlighter peak $h\nu$ of 1 keV), the optical depth is proportional to areal density.

The evolution of the unperturbed and 2D targets was modeled with the 2D code LASNEX (Zimmerman & Kruer 1975) , and that of the 3D targets with the 3D code HYDRA(Marinak et al. 1996). The simulations were used to predict radiographs which included the transmission of x-ray backlighters and the diagnostic resolution. The Fourier transforms of the 2D simulated and measured radiographs give a modulation amplitude of the fundamental and harmonics in areal density, and the comparison is shown in Figures 5b-d for the various wavelengths. The data agree with the simulations except in the case of the 50 μm wavelength, where the absolute timing does not agree (data

are about 200 ps earlier than the simulation). The absolute timing is determined by timing shots and fiducial pulses, with an uncertainty of 150 ps.

The simulated and measured 3D radiographs at t=6 ns are shown in Figure 6a and 6b (the gray scale covers the same range in optical depth in both cases). A more quantitative comparison of the 3D data with the simulation is obtained by extracting the 2D Fourier spectrum of the data and the simulations as a function of time. The two-dimensional power spectra (with mode zero at the center) were averaged for values of mode number |m|, i.e.

$$P(m) = \left[\frac{\sum_{0}^{n} \left[T(|m|, \theta) \right]^2}{n} \right]^{1/2} \qquad (1)$$

where P is the power spectrum, T is the Fourier transform of τ, |m| is the magnitude of the mode number (300 μm/wavelength in μm), and θ is the angle in Fourier space. When the Fourier transform is converted from Cartesian to polar coordinates, modes with $m-0.5<m\leq m+0.5$ are taken to be mode m. The azimuthal averages of the two-dimensional power spectra, averaged over all the frames at one time, for the data and the simulations are shown in Figure 7. The simulated spectra agree with the data as a function of time. Both the data and simulation show the peak of the Fourier spectrum has devel-

oped at mode 4 (75 μm wavelength), slightly below the peak of the growth factor spectrum.

II. Two-dimensional spherically convergent experiment

The convergent geometry experiments examined the evolution of sinusoidal ripples on a capsule, as described above. Time sequences of images, taken with the x-ray framing camera with 50 ps frame time and an MTF as shown above are shown in Fig. 8. The perturbation for the hemisphere corresponded to an initial 300 x 300 micron square patch with 70 micron wavelength, 2 micron amplitude sinusoidal ripple imposed on it. This rippled patch was constructed using the excimer laser, in the same fashion as the mold for the 3D pattern. Each capsule must be ablated to produce the ripples, as a mold cannot be used on the spherical surface. Shock breakout is at about 1.4 ns, and as the hemisphere accelerates from 1.5-2.25 ns, it also converges by over a factor of two, as seen by the shrinking of the imposed perturbation patch. The 2D simulations (Cherfils et al. 1997) using the code FCI2 show that for convergences of up to a factor of 2, the implosion is reasonably spherical. Hence, the observed convergence translates to an acceleration history. The data are analyzed as were the planar data. The 2D simulations were post-processed to include the transmission of the backlighter along the line of sight through the spherical simulation and the effect of the instrument MTF. The Fourier analysis of the data is shown in Fig. 9. The roll-over immediately following

the observed peak in growth factor is partly an instrumental effect, because the instrument modulation transfer function (MTF) drops as the fundamental wavelength decreases due to convergence. The 2D simulations for the convergent experiments give quite good agreement with the data, as shown in Fig. 9.

Rayleigh-Taylor instabilities at a photoevaporation front may be an astrophysical equivalent to the RT instabilities we have been describing in these proceedings. In 1954 (Frieman 1954; Spitzer 1954) it was suggested that the gaseous pillars in M16 might have been formed through a Rayleigh-Taylor instability. While the current understanding of these structures is that they are formed by the shadowing of material from ultraviolet ablation by globules in the initial nebula, not by the RT instability (Bertoldi 1989), it is still likely that the RT instability plays a role in the evolution of the photoevaporation front. The parameters of the photoevaporation and photoionization fronts have been calculated by Hester et al.(Hester et al. 1996) and are reproduced in Figure 10. The density and temperature (and, hence, pressure) profiles are seen to show the increase of density and decrease in pressure which characterize a RT unstable interface. The plasma, created by photoevaporation and photoionization by nearby stars (drive temperature ~50 000 K) is inferred to have a peak density of about 2400 cm^{-3}, decaying with a scale length of about 5×10^{16} cm. The temperature and thus the pressure scale length is about 1×10^{16}

cm. The expression for RT growth rate of modes with wave number smaller than the inverse of the pressure scale length is (Bandiera 1984)

$$\sigma_c^2 = \left(P^2 - \gamma PR\right)c_s^2 / \gamma^2$$

in which σ_ζ is the growth rate, γ is the adiabatic gas constant, c_s is the sound speed (~ 10^6 cm/s), $P = \frac{\partial \ln(p)}{\partial r} = 1/(1\times10^{16}$ cm), and $R = \frac{\partial \ln(\rho)}{\partial r} = 1/(5\times10^{16}$ cm). Thus, $\sigma_\zeta \sim 10^{-10}$ s^{-1} (on the order of 10^3 years for one e-folding). Perturbations of $>10^{16}$ cm would be expected to show growth (the pillars are about 1 pc, or 3×10^{18} cm, long).

The difference between the conditions at the photoevaporation front in gaseous nebulae such as M16 and the ablation front in laser-driven experiments is primarily one of scale. This question is addressed by Ryutov (Ryutov 1998),and the RT growth at the ablation front is found to be invariant under a scale transformation which preserved the quantity $L/[(P_a/\rho)^{1/2}\tau]$, where L is the characteristic spatial scale, P_a is the ablation pressure, ρ is the density, and τ is the time scale. For the M16 pillars, the pressure at the photoionization front is about 8.7×10^7 cm^{-3} K *k, where k is Boltzmann's constant (Pound 1998), and the density is 2000 cm^{-3}. At the ablation front in the Nova experiments, Pa is 10 Mbar and ρ is about 5 gm/cm^3. Thus 2×10^{11} seconds in the M16 conditions corresponds to 2 ns in the laser-driven experiments.

In conclusion, we have described a number of experiments which, using the intense Nova laser facility, examined the growth of a Rayleigh-Taylor unstable ablation front. Our experiments have been well modeled with two- and three-dimensional radiation hydrodynamics codes. Conditions in these experiments are similar (at a much larger scale) to those existing in photoionizing clouds such as those in the Eagle nebula pillars, suggesting that codes which model the behavior of these nebulae could with some modification be benchmarked against these and other well-understood laser driven ablation front experiments.

This work was performed under the auspices of the U.S. DOE by LLNL under contract No. W-7405-Eng-48.

Figure captions.

1. Schematic of the experiments, showing position of ablated foils or capsules on hohlraum wall and backlighting geometry.

Figure 2. Schematic of an x-ray framing camera.

Figure 3. Backlighter spectra from laser-produced plasmas as used in the Nova experiments for a) Sc and b) Rh targets.

Figure 4. Laser power (left axes, light gray) and resulting hohlraum blackbody temperature (right axes, dark gray) for a) the planar and b) the convergent geometry experiments.

Figure 5. Radiographs of target foils with three-dimensional pattern, a) as designed and b) as measured.

Figure 6. Results from planar experiment with (a) no modulation and with two-dimensional sinusoidal modulations of various wavelengths: (b) 30 μm, (c) 50 μm, and (d) 100 μm.

Figure 7. Simulated (a) and measured (b) radiographs of the three-dimensional rippled foil after 6 ns of growth.

Figure 8. Comparison of simulated and measured Fourier spectra at various times.

Figure 9. Measured radiographs of the convergent target at t= 1.55, 1.80, 1.99, and 2.18 ns.

Figure 10. Simulated and measured first and second Fourier harmonics versus time for the convergent experiments.

Figure 11. Gaseous pillars in M16.

Figure 12. Simulations from Hester 1996 of density and temperature profiles in the photoionization front in M16.

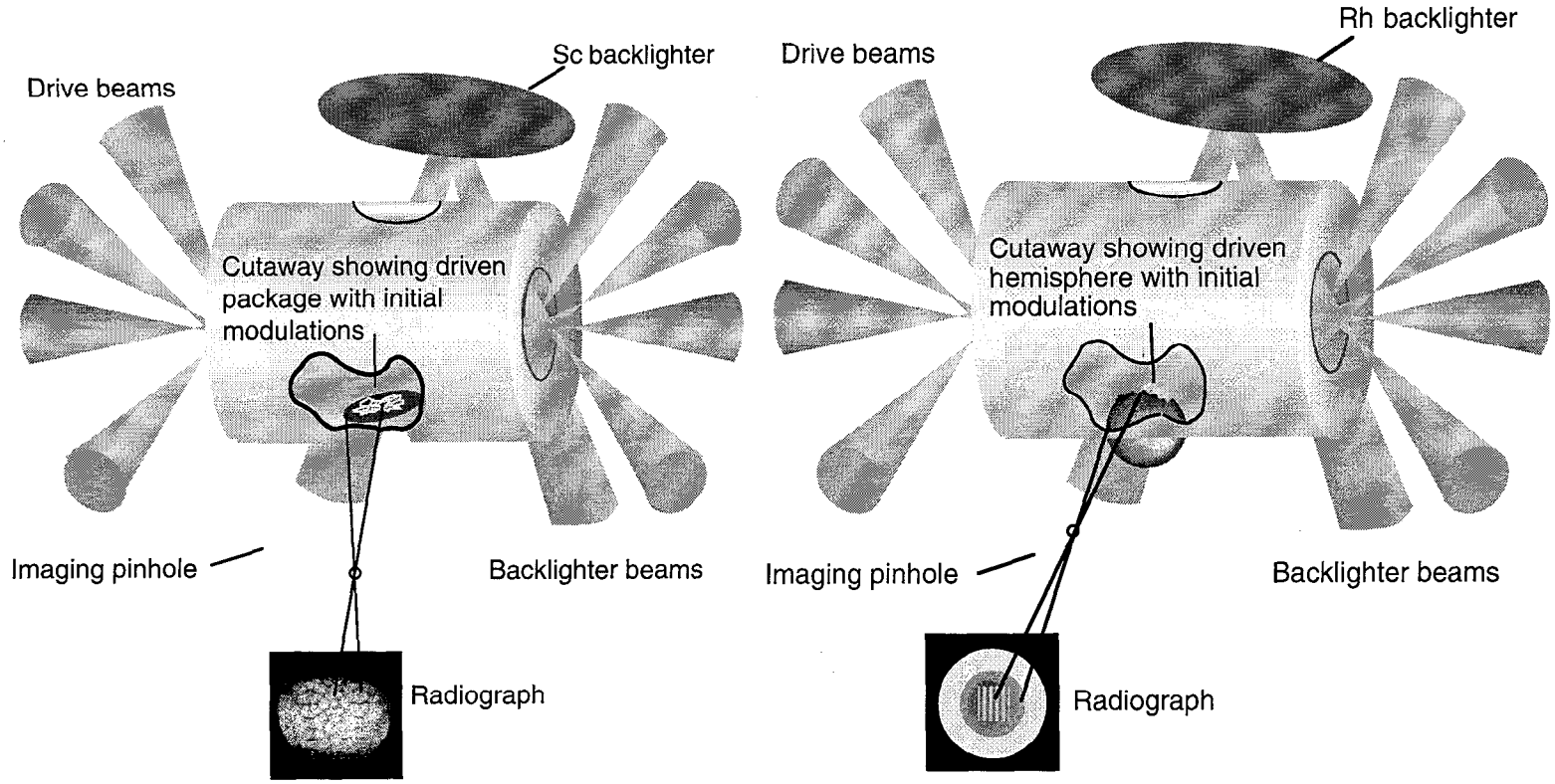
Drive beams
Sc backlighter
Cutaway showing driven package with initial modulations
Imaging pinhole
Backlighter beams
Radiograph
Drive beams
Rh backlighter
Cutaway showing driven hemisphere with initial modulations
Imaging pinhole
Backlighter beams
Radiograph

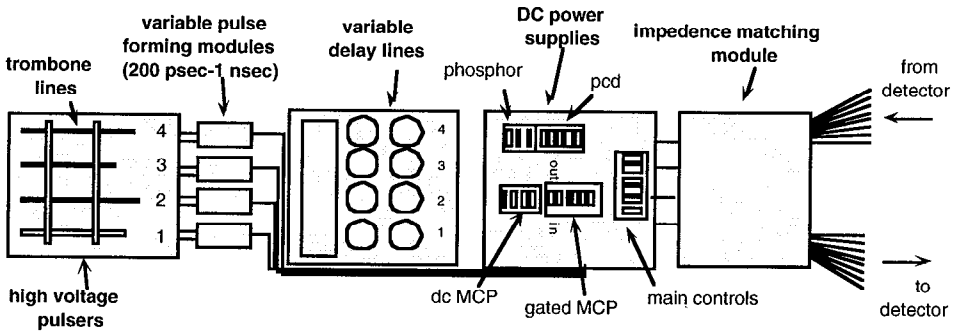

view from side:
GXI snout

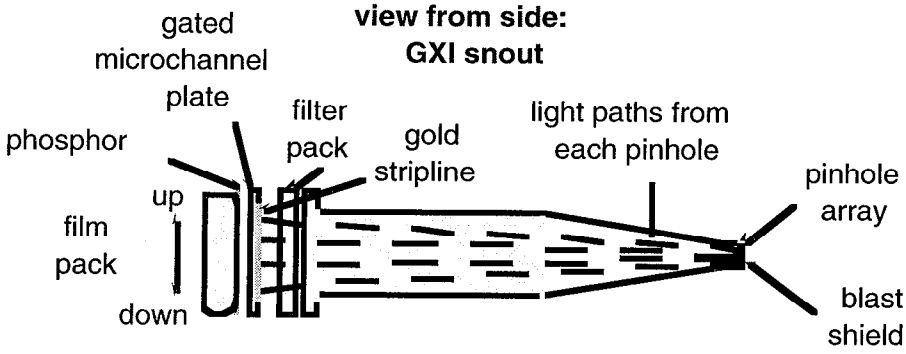

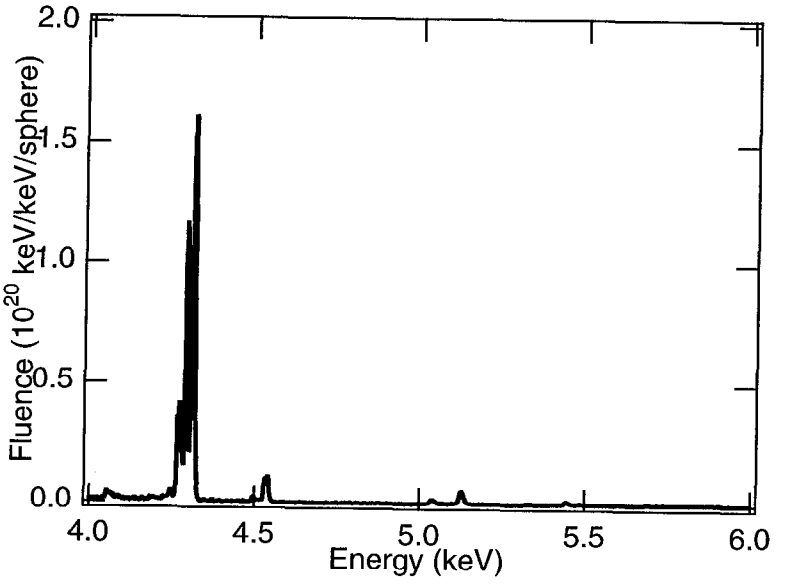
2.0
1.5
1.0
0.5
0.0
Fluence (10^{20} keV/keV/sphere)
4.0
4.5
5.0
5.5
6.0
Energy (keV)

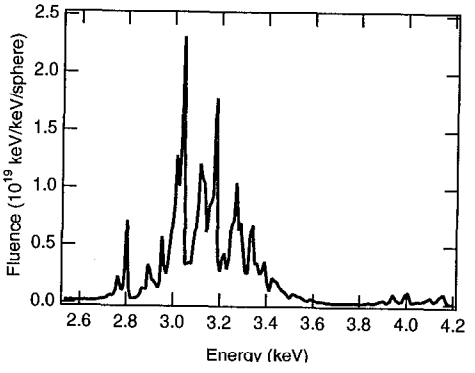
2.5
2.0
1.5
1.0
0.5
0.0
Fluence (10^{19} keV/keV/sphere)
2.6
2.8
3.0
3.2
3.4
3.6
3.8
4.0
4.2
Energy (keV)

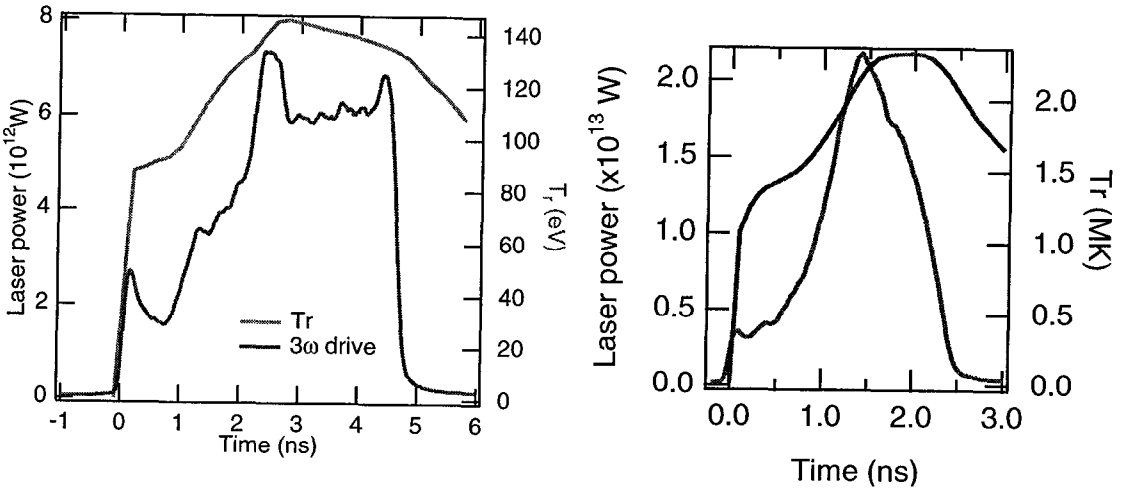
Laser power (10^{12}W)
T_r (eV)
Time (ns)
Tr
3ω drive
Laser power (x10^{13} W)
Tr (MK)
Time (ns)

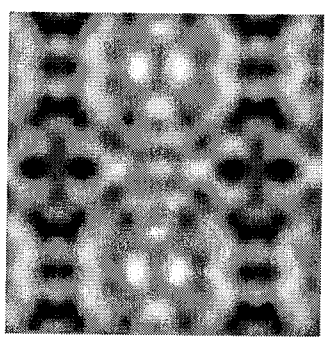

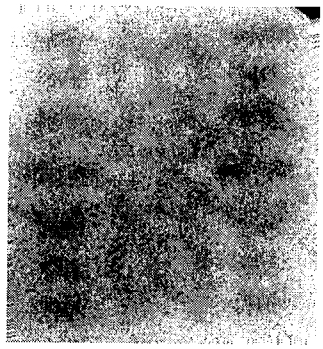

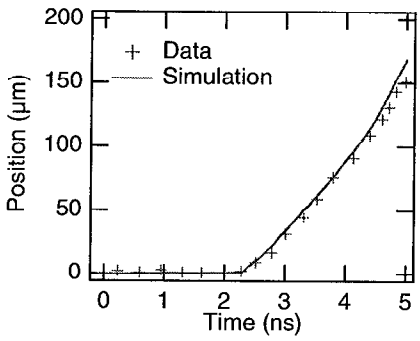
Position (μm)
200
150
100
50
0
Data
Simulation
0 1 2 3 4 5
Time (ns)

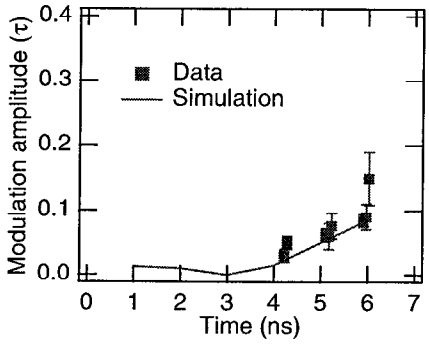
Modulation amplitude (τ)
0.4
0.3
0.2
0.1
0.0
Data
Simulation
0 1 2 3 4 5 6 7
Time (ns)

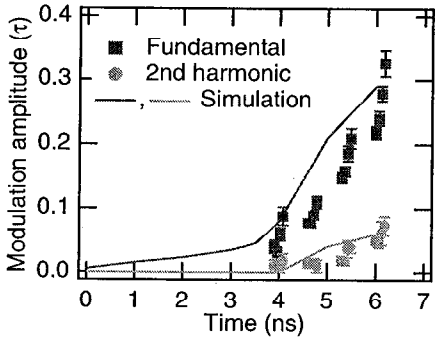
Modulation amplitude (τ)
0.4
0.3
0.2
0.1
0.0
Fundamental
2nd harmonic
Simulation
0 1 2 3 4 5 6 7
Time (ns)

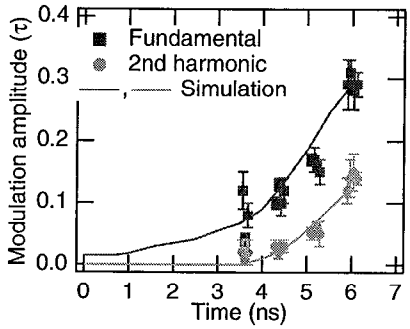
Modulation amplitude (τ)
0.4
0.3
0.2
0.1
0.0
Fundamental
2nd harmonic
Simulation
0 1 2 3 4 5 6 7
Time (ns)

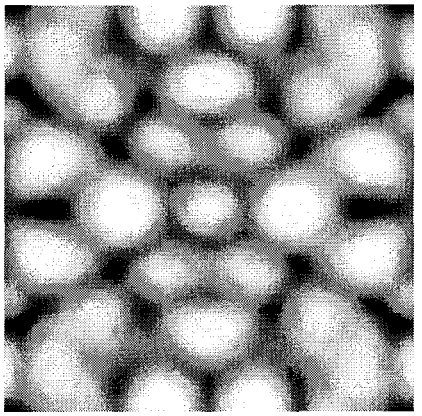

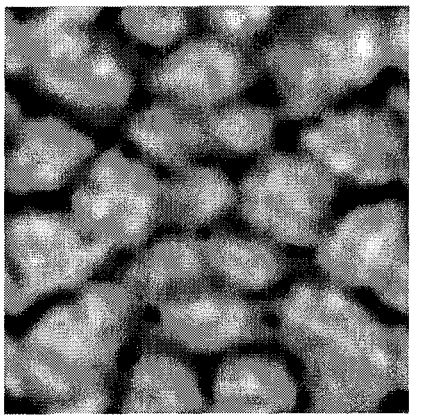

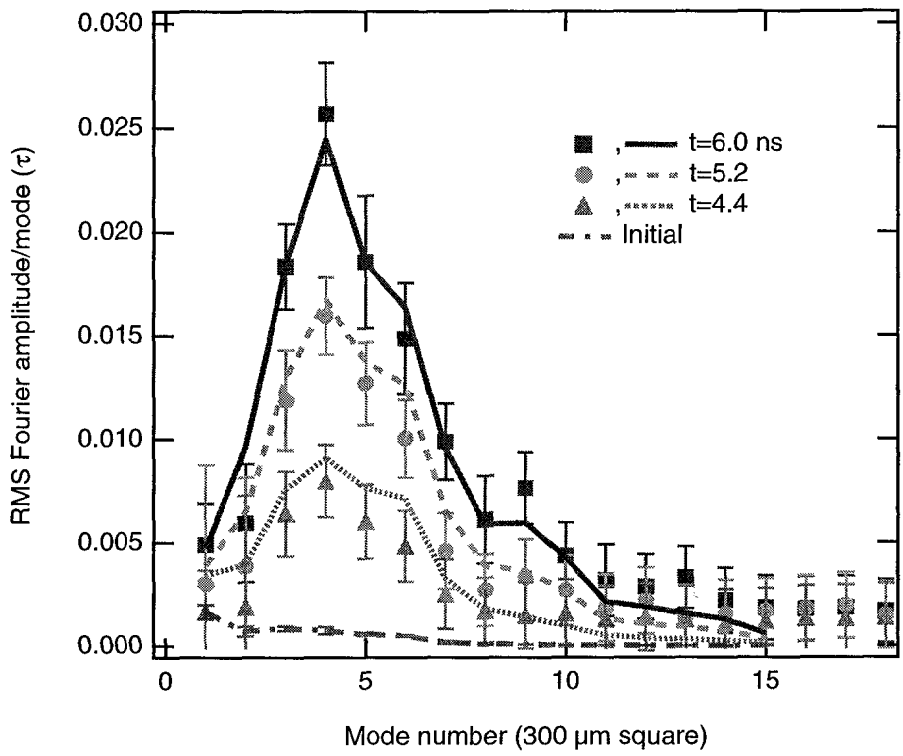
0.030
0.025
0.020
0.015
0.010
0.005
0.000
0
5
10
15
RMS Fourier amplitude/mode (τ)
Mode number (300 μm square)
t=6.0 ns
t=5.2
t=4.4
Initial

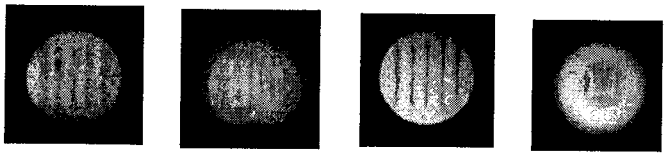

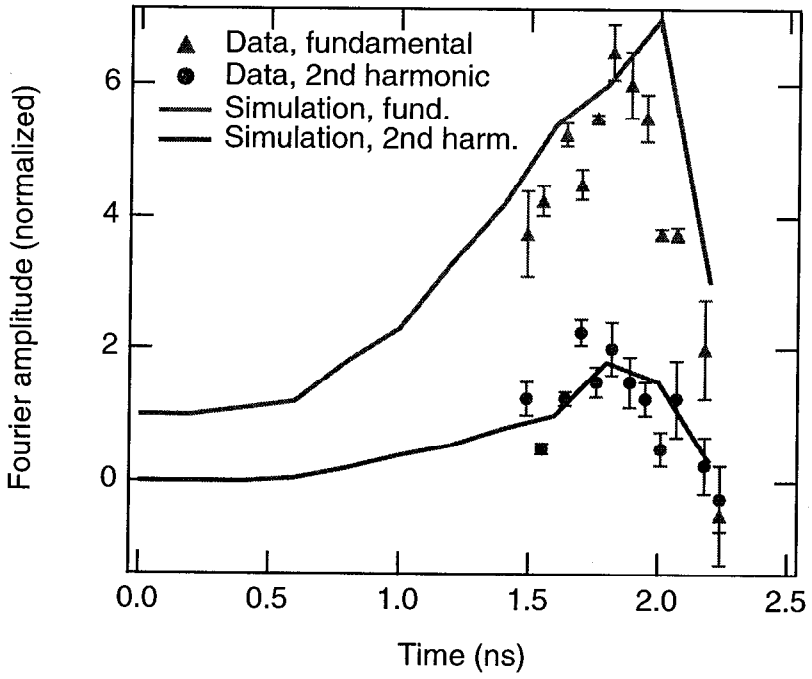
Data, fundamental
Data, 2nd harmonic
Simulation, fund.
Simulation, 2nd harm.
Fourier amplitude (normalized)
0
2
4
6
0.0
0.5
1.0
1.5
2.0
2.5
Time (ns)


Gaseous Pillars • M16
HST • WFPC2
J. Hester and P. Scowen (AZ State Univ.), NASA

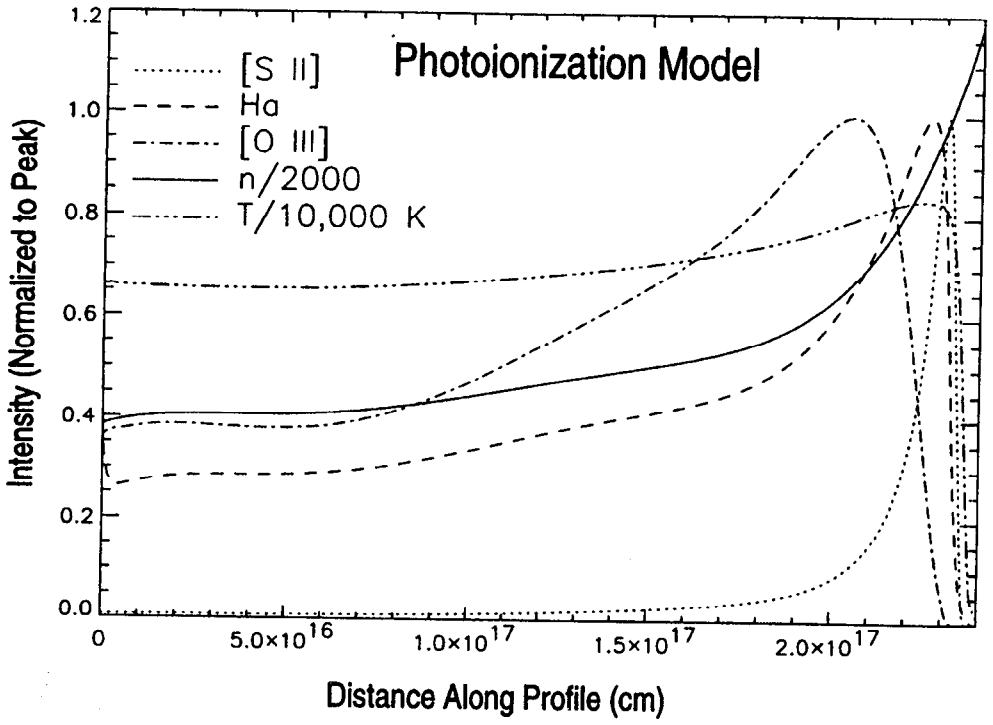
Photoionization Model
[S II]
Hα
[O III]
n/2000
T/10,000 K
Intensity (Normalized to Peak)
1.2
1.0
0.8
0.6
0.4
0.2
0.0
0
5.0×10^16
1.0×10^17
1.5×10^17
2.0×10^17
Distance Along Profile (cm)

Bandiera, R. 1984, Astronomy and Astrophysics, 139, 368

Bertoldi, F. 1989, Astrophysical Journal, 346, 735

Bradley, D. K., Bell, P. M., Landen, O. L., Kilkenny, J. D. & Oertel, J. 1995, Review of Scientific Instruments, 66, 716

Cherfils, C., Galmiche, D., Richard, A., Glendinning, S. G. & Remington, B. A. (1997). Numerical investigation of convergent Rayleigh-Taylor Experiments on the Nova laser. Sixth International Workshop on the Physics of Compressible Turbulent Mixing, Marseilles, France, Imprimerie Caractère,

Endo, T., Shigemori, K., et al. 1995, Physical Review Letters, 74, 3608

Frieman, E. A. 1954, Astrophysical Journal, 120, 18

Glendinning, S. G., Landen, O. L., Remington, B. A. & Hammel, B. A. (1995). Laser plasma diagnostics of dense plasmas. Applications of Laser Plasma Radiation II. Bellingham, WA, SPIE. **2523:** 29.

Glendinning, S. G., Weber, S. V., et al. 1992, Physical Review Letters, 69, 1201

Hester, J. J., Scowen, P. A., et al. 1996, Astronomical Journal, 111, 2349+

Hsing, W. W., Barnes, C. W., et al. 1997, Physics of Plasmas, 4, 1832

Kilkenny, J. D., Glendinning, S. G., et al. 1994, Physics of Plasmas, 1, 1379

Landen, O. L., Keane, C. J., et al. 1996, Physics of Plasmas, 3, 2094

Marinak, M. M., Tipton, R. E., et al. 1996, Physics of Plasmas, 3, 2070

Nuckolls, J., Wood, L., Thiessen, A. & Zimmerman, G. 1972, Nature, 239, 139

Pawley, C. J., Gerber, K., et al. 1997, Physics of Plasmas, 4, 1969

Remington, B. A., Haan, S. W., et al. 1992, Physics of Fluids B-Plasma Physics, 4, 967

Remington, B. A., Hammel, B. A., Landen, O. L. & Pasha, R. A. 1992, Review of Scientific Instruments, 63, 5083

Robey, H. F., Budil, K. S. & Remington, B. A. 1997, Review of Scientific Instruments, 68, 792

Ryutov, D. (1998). An attempt to establish similarity criteria in the hydrodynamics of indirectly-driven ablation fronts.

Spitzer, L. 1954, Astrophysical Journal, 120, 18

Wallace, R. J., McEachern, R. L. & Wilcox, W. W. (1994). ICF Capsule Fabrication by Laser Ablation. Livermore, Lawrence Livermore National Laboratory. 79.

Weber, S. V., Remington, B. A., Haan, S. W., Wilson, B. G. & Nash, J. K. 1994, Physics of Plasmas, 1, 3652

Zimmerman, G. B. & Kruer, W. L. 1975, Comments on Plasma Physics and Controlled Fusion, 2, 51